J Biol Inorg Chem (2007) 12:1097–1105
DOI 10.1007/s00775-007-0281-3

ORIGINAL PAPER

Two sub-states of the red2 state of methyl-coenzyme M reductase revealed by high-field EPR spectroscopy

Denise I. Kern · Meike Goenrich · Bernhard Jaun · Rudolf K. Thauer · Jeffrey Harmer · Dariush Hinderberger

Received: 18 May 2007 / Accepted: 18 July 2007 / Published online: 10 August 2007

Abstract Methyl-coenzyme M reductase (MCR) catalyzes the formation of methane from methyl-coenzyme M and coenzyme B in methanogenic archaea. The enzyme has two structurally interlinked active sites embedded in an $\alpha_2\beta_2\gamma_2$ subunit structure. Each active site has the nickel porphyrinoid F_{430} as a prosthetic group. In the active state, F_{430} contains the transition metal in the Ni(I) oxidation state. The active enzyme exhibits an axial Ni(I)-based continuous wave (CW) electron paramagnetic resonance (EPR) signal, called red1a in the absence of substrates or red1c in the presence of coenzyme M. Addition of coenzyme B to the MCR-red1 state can partially and reversibly convert it into the MCR-red2 form, which shows a rhombic Ni(I)-based EPR signal (at X-band microwave frequencies of approximately 9.4 GHz). In this report we present evidence from high-field/high-frequency CW EPR spectroscopy (W-band, microwave frequency of approximately 94 GHz) that the red2 state consists of two substates that could not be resolved by EPR spectroscopy at X-band frequencies. At W-band it becomes apparent that upon addition of coenzyme B to MCR in the red1c state, two red2 EPR signals are induced, not one as was previously believed. The first signal is the well-characterized (ortho)rhombic EPR signal, thus far called red2, while the second previously unidentified signal is axial. We have named the two substates MCR-red2r and MCR-red2a after their rhombic and axial signals, respectively.

Keywords Methyl-coenzyme M reductase · Nickel enzyme · Factor F_{430} · Methanogenic archaea · Electron paramagnetic resonance spectroscopy

Abbreviations

CH_3-S-CoM	Methyl-coenzyme M
CW	Continuous wave
EPR	Electron paramagnetic resonance
HS-CoB	Coenzyme B
HS-CoM	Coenzyme M
HYSCORE	Hyperfine sublevel correlation
MCR	Methyl-coenzyme M reductase

Introduction

Methyl-coenzyme M reductase (MCR) catalyzes the reduction of methyl-coenzyme M [CH_3-S-CoM; (2-methyl-mercaptoethanesulfonate)] with coenzyme B [HS-CoB; (*N*-7-mercaptoheptanoylthreonine phosphate)] to methane

Electronic supplementary material The online version of this article (doi:10.1007/s00775-007-0281-3) contains supplementary material, which is available to authorized users.

D. I. Kern · J. Harmer · D. Hinderberger
Laboratorium für Physikalische Chemie,
ETH Zürich,
Wolfgang-Pauli-Strasse 10,
8093 Zurich, Switzerland

D. Hinderberger (✉)
Max-Planck-Institut für Polymerforschung,
Ackermannweg 10,
55128 Mainz, Germany
e-mail: hinderberger@mpip-mainz.mpg.de

B. Jaun
Laboratorium für Organische Chemie,
ETH Zürich,
Wolfgang-Pauli-Strasse 10,
8093 Zurich, Switzerland

M. Goenrich · R. K. Thauer
Max-Planck-Institut für Terrestrische Mikrobiologie,
Karl-von-Frisch-Straße,
35043 Marburg, Germany

and the heterodisulfide CoM-S-S-CoB, which is the key step of methanogenesis in archaea (Eq. 1, Fig. 1):

$$\begin{aligned} &CH_3\text{-S-CoM} + \text{HS-CoB} \rightarrow CH_4 + \text{CoM-S-S-CoB} \\ &\Delta G^{0'} = -30\,\text{kJ}\,\text{mol}^{-1}. \end{aligned} \quad (1)$$

Methanogenic archaea are found in strictly anoxic environments, e.g., swamps, freshwater sediments, sewage sites or the rumen and guts of animals [1], and they gain the energy necessary for ATP synthesis by producing methane from substrates such as H_2/CO_2, acetate, formate or methanol [1, 2]. Globally, methane generated from the metabolic activity of archaea amounts to an estimated 10^9 t annually, with approximately half of this very effective greenhouse gas being released into earth's atmosphere. All methanogens contain MCR, which has a molecular mass of approximately 300 kDa and consists of three different types of subunits in a hexameric $\alpha_2\beta_2\gamma_2$ arrangement. Each molecule of the enzyme contains two molecules of the cofactor F_{430}, a nickel porphyrinoid [1, 3], as the prosthetic group. From X-ray crystallography of inactive Ni(II) forms (from *Methanothermobacter marburgensis*) it is known that the enzyme has two identical active sites, each containing one molecule of factor F_{430} (Fig. 1) located about 5.1 nm apart, each situated at the bottom of a 5.0 nm long channel. The reaction center is enclosed by hydrophobic aromatic residues.

The active MCR-red1 state has the central metal in the Ni(I) oxidation state and its continuous wave (CW) electron paramagnetic resonance (EPR) spectrum is characteristic of a d^9 S = 1/2 species with the unpaired electron in a molecular orbital of predominantly nickel $d_{x^2-y^2}$ character [4]. Three forms of MCR-red1 are known: MCR-red1a, in the absence of any substrates; MCR-red1m, in the presence of CH_3-S-CoM; and MCR-red1c, in the presence of coenzyme M (HS-CoM; 2-mercaptoethanesulfonate). All three states have in common an axial EPR spectrum, i.e., two g values (g_x, g_y) are very similar and one value (g_z) is significantly different [1].

HS-CoM acts as a competitive inhibitor for MCR. In the catalytic reaction cycle, the substrate CH_3-S-CoM accesses the active site through the narrow channel. Despite a wealth of experimental and computational data, the interaction between CH_3-S-CoM and the nickel in the catalytic cycle of MCR is still a matter of discussion. Of the two currently most favored proposed reaction mechanisms, one corresponds to an attack of Ni(I) on the sulfur of CH_3-S-CoM resulting in an intermediate with a Ni–S bond, whereas the other consists of an attack of Ni(I) on the carbon of the methyl group giving a Ni–CH_3 bond intermediate [1, 5, 6].

Except for MCR with bound HS-CoM (red1c), at X-band (approximately 9.4 GHz), the CW EPR spectra of MCR-red1 species show well-resolved hyperfine splitting stemming from the four-coordinated (porphyrin) nitrogen. This may indicate that the geometry is less well defined for red1c, which may blur the hyperfine structure [7].

A drastic change in the EPR signal is induced by addition of HS-CoB to MCR-red1c: a certain percentage of the signal changes from an axial to the (ortho)rhombic red2 signal. Hyperfine sublevel correlation (HYSCORE) and CW EPR studies on this red2 state induced with H^{33}S-CoM showed that it is associated with reversible binding of the sulfur of HS-CoM to the Ni(I) ion. It has been suggested that there is a conformational change which allows the thiol moiety of HS-CoM to coordinate the Ni(I) ion. Such a change in conformation potentially also occurs during catalysis, i.e., upon addition of HS-CoB to MCR-red1m. In all experiments so far the maximum amount of conversion of red1c into red2 has been less than 50% [8].

Building on an initial study [8], our goal was to characterize the conversion of MCR from the red1c state to the red2 state in more detail, in particular its temperature dependence and the fact that at X-band at most 50% of the initial red1c signal is converted to the red2 signal. We have previously found that the conversion of the MCR-red1c state to the MCR-red2 state upon addition of HS-CoB is reversible and seems to be thermodynamically unfavorable at temperatures below 20 °C. This correlates with the methane-formation ability of MCR in the presence of CH_3-

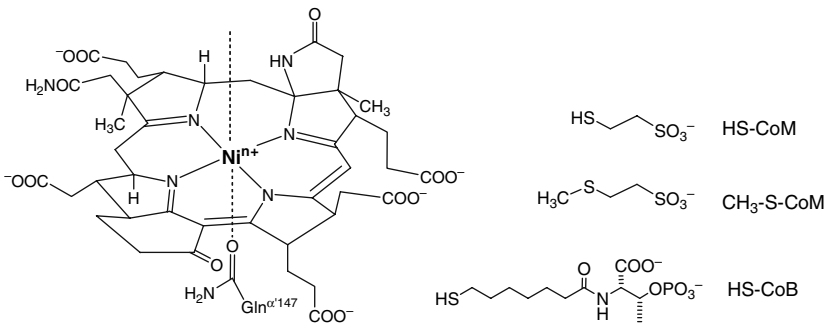

Fig. 1 Molecular structures of the nickel porphyrinoid F_{430} [for Ni(III): n = 2] and the substrates methyl-coenzyme M (*CH_3-S-CoM*) and coenzyme B (*HS-CoB*). Addition of the substrate analogue coenzyme M (*HS-CoM*) leads to the methyl-coenzyme M reductase (MCR) red1c state

S-CoM and HS-CoB, which is only observable at significant rates at temperatures above 20 °C. These findings (among others, see [8, 19, 20]) have led us to propose the red2 state as a model for an intermediate state of active MCR. In this work, we used high-field EPR spectroscopy (at W-band with a tenfold increased magnetic field and frequency), with its significantly improved resolution compared with X-band to investigate the red1/red2 states of MCR in more detail.

Materials and methods

M. marburgensis (*M. thermoautotrophicum*, strain Marburg [9]) is the strain deposited under DSM 2133 in the Deutsche Sammlung von Mikroorganismen und Zellkulturen (Braunschweig). HS-CoM was obtained from Merck (Darmstadt). CH_3-S-CoM was synthesized from HS-CoM by methylation with methyl iodide (Fluka) [7, 10]. HS-CoB was prepared from the symmetric disulfide CoB-S-S-CoB by reduction with $NaBH_4$ [11, 12].

Purification of active MCR

M. marburgensis was grown at 65 °C in a 13-L glass fermenter (New Brunswick) containing 10 L mineral medium stirred at 1,200 rpm and gassed with 80% H_2/20% CO_2/0.1% H_2S at a rate of 1,200 mL min^{-1} [7]. When a difference in optical density at 578 nm of 4.5 was reached, the gas supply was switched to 100% H_2 for 30 min to induce the EPR signals of MCR-red1 and MCR-red2 in the cells. After 30 min the cells were cooled to 10 °C within 10 min under continuous gassing and harvested anaerobically by centrifugation using a flow-through centrifuge (Hettich, centrifuge 17 RS). Approximately 70 g of wet cells was obtained. From these cells only the MCR isoenzyme I was purified [13, 14]. All steps of the purification were performed in the presence of 10 mM HS-CoM and in an anaerobic chamber (Coy Instruments) filled with 95% N_2/5% H_2 as described previously [7]. During purification the enzyme lost its MCR-red2 signal owing to the removal of HS-CoB. In one purification generally 150 mg active MCR in the red1c state (in 10 mL) was obtained. The purified enzyme exhibited a greenish color and showed a UV–vis spectrum at room temperature with a maximum at 385 nm (ε = 54,000 M^{-1} cm^{-1}), and an axial EPR signal with g_z = 2.25, g_y = 2.07 and g_x = 2.06 characteristic for MCR-red1c [7, 15, 16]. The protein concentration was determined using the method of Bradford [17] with bovine serum albumin (Serva) as a standard or by measuring the absorbance difference of oxidized enzyme (MCR-silent) at 420 nm using ε = 44,000 M^{-1} cm^{-1} for a molecular mass of 280,000 Da. Both methods yielded almost the same results.

EPR spectroscopy

To check for their EPR activity, samples were first routinely analyzed by X-band EPR spectroscopy at −196 °C in 3-mm inner diameter, 0.35-mL quartz tubes with 95% N_2/5% H_2 as the gas phase and closed with a closed-off rubber tube (data not shown).

The EPR spin quantitations were carried out under nonsaturating conditions using 10 mM copper perchlorate as the standard (10 mM $CuSO_4$, 2M $NaClO_4$, 10 mM HCl). All signal intensities are expressed as spin concentrations per mole of F_{430}. Note that accurate absolute spin quantitation is difficult to achieve, so the spin concentrations obtained have an error of at least 10%. The samples were obtained with an electron spin concentration of approximately 0.75 per mole F_{430}, amounting to approximately 1.5 mM. The content of MCR in silent states is thus approximately 25%.

W-band sample tubes had an outer diameter of 0.7 mm and all samples were stored in liquid nitrogen. To protect the samples from oxidation the tubes were sealed after evacuation to 5–6 × 10^{-6} mbar at liquid nitrogen temperature. The samples were evacuated in a freeze–pump–thaw procedure that was repeated two to three times where the temperature of the samples was briefly allowed to rise (while under vacuum) in order to thaw them and subsequently remaining traces of oxygen were removed. Precautions were taken to ensure that the bulk of the sample remained frozen at all times.

For the measurements of incubation temperature dependent spectra, the now-sealed W-band sample tubes were prepared as follows.

1. The samples were always thawed to room temperature.
2. Then they were incubated for 3–4 min in a water bath or an ethanol bath with a temperature ranging from −21 to 40 °C. In addition to always thawing the sample tubes, the order of the incubation temperatures was chosen arbitrarily (i.e., we did not start with −21 °C and go stepwise to 40 °C or vice versa but we chose a random order of the incubation temperatures) to exclude artifacts from hidden trends.
3. Freeze–quench was performed by inserting the sample from the bath at the incubation temperature directly into ethanol at temperatures below −100 °C (viscous limit). After this step, the samples remained frozen until all EPR experiments had been finished.
4. To remove the highly viscous ethanol sticking to the sample tube, the tubes were then briefly dipped in

ethanol at approximately −50 °C and quickly wiped with a tissue, put into liquid nitrogen and inserted into the probehead at −213 °C.

After the EPR measurements had finished, the sample tube was removed from the probehead and the sample preparation procedure was resumed at step 1, now choosing a different incubation temperature in step 2. All CW EPR spectra were recorded using a Bruker ElexSys E680 spectrometer at W-band. The microwave frequencies varied between 94.09 and 94.19 GHz, and spectra were recorded with a modulation frequency of 100 kHz and a modulation amplitude of 0.7 mT.

Data processing

All spectral simulations as well as data processing were performed with home-written programs in MATLAB 6.5 (The MathWorks) employing the EasySpin toolbox [18]. The CW EPR spectra were simulated as a superposition of the frozen solution (powder) simulations of all species present in the sample (Fig. 2) and the background consisting of a baseline correction with zero-, first- and second-order polynomials and a corresponding simulation of the probehead background stemming from a radical of unknown origin.

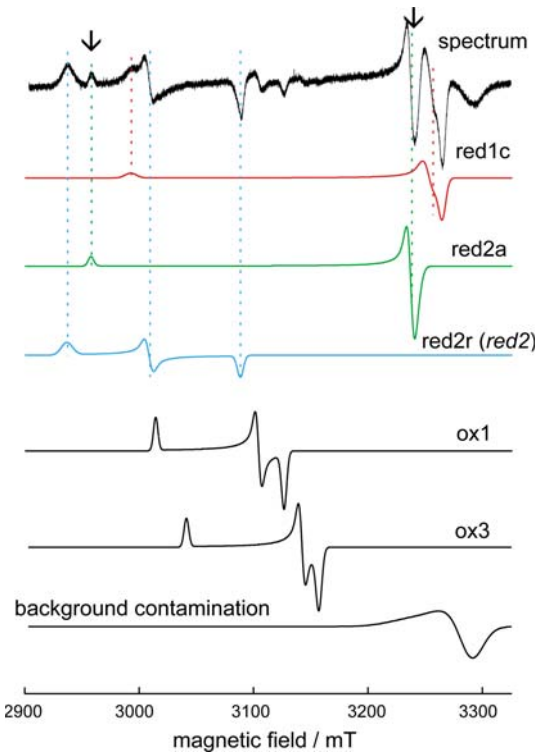

Fig. 2 Continuous wave (CW) electron paramagnetic resonance (EPR) spectrum of MCR in the red1/red2 states at W-band (*top*, microwave frequency 94.12 GHz) and spectral simulation of all individual components. The background signal of the probehead is of unknown origin. The *dashed lines* are meant as guides for the eye

The simulation was fitted to the recorded spectra using the least-squares operator "\" to yield the optimized weights, i.e., the relative integral contribution to the overall spectrum. For an optimized simulation the linewidth was adjusted through the *H* strain values (unresolved hyperfine splitting) to fit experimental data. For data analysis and interpretation purposes, the probehead component was subtracted and the remaining weights were normalized to unity. The weights were found not to be very sensitive to *g* and *H* values. Slight variation of parameters (e.g., Δg = 0.005) resulted in a maximum difference of 2 wt%.

Results

To achieve better characterization of MCR in the red1c/red2 state, we used high-field EPR spectroscopy (at W-band). Figure 2 displays a typical W-band CW EPR spectrum (top row, measured at −213 °C) of MCR that was supplied with HS-CoM and HS-CoB and that was incubated at 40 °C prior to freezing.

Figure 2 also features spectral simulations of the different components that contribute to the overall signal (the *g* values are in good agreement with previously reported values [20] and are summarized in Table 1).

Owing to improved *g* resolution, all spectral components are resolved: the states red1c (showing an almost axial signal) and red2 [hereafter labeled red2r, showing a clearly (ortho)rhombic spectrum] are present, which is to be expected due to the HS-CoM plus HS-CoB preparation. Also, the states ox1 and ox3, which are formed either during growth of the cell cultures by gassing with less reducing gas mixtures or supplying Na_2S (ox1) or by the presence of oxygen (ox3), could be identified [1, 16], both displaying rhombic EPR signals. However, there is one new spectral component which is clearly resolved at W-band (marked by arrows). One additional peak is apparent between the g_x feature (at the low-field end of the spectrum) of red2r and the g_z component of red1c. The other feature becomes apparent at slightly lower magnetic field than the g_x/g_y–peak of red1c. Similarly to the (ortho)rhombic signal red2r, this new axial EPR signal is only observed after addition of HS-CoM *and* HS-CoB to active MCR (further proof will be provided in the course of the paper). In addition, this newly discovered spectral component also shows a temperature-dependent induction behavior similar to that of the red2 state. Hence, we call this state the *red2a* ("red2axial") state and refer to the initial red2 state as *red2r* ("red2rhombic").

Close inspection of the red2a *g* values (g_x = 2.0750, g_y = 2.0775, g_z = 2.2740) clearly shows why this spectral

Table 1 g values for the electron paramagnetic resonance (EPR) signals of the individual states of methyl-coenzyme M reductase obtained from simulation of the continuous wave EPR spectra at W-band

	red1c	red2r	red2a	ox1	ox3	Contamination
g_x	2.0600	2.2900	2.0750	2.1510	2.2110	2.0460
g_y	2.0680	2.2355	2.0775	2.1665	2.1400	2.0520
g_z	2.2475	2.1780	2.2740	2.2310	2.1300	2.0780

The margin of error is $\Delta g = \pm 0.0005$

component could not be detected as an individual signal at X-band (approximately 9.4 GHz) frequencies. Although at Q-band (approximately 35 GHz) frequencies the red2a peaks start being resolved, a clear-cut assignment to an individual species is almost impossible. This furthermore explains the observation at X-band that the "red1" component in MCR-red1/red2 seemed to have slightly higher g values than red1c: upon addition of HS-CoB also the red2a signal is induced and overlaps with the red1c signal, giving the impression that there is a signal with g values that are shifted to higher values compared with those of red1c. The g matrix of the red2a species is almost axial and—assuming a similar electronic ground state as red1c (nickel $d_{x^2-y^2}$)—displays only a slight (ortho)rhombicity in the g_x and g_y values.

Temperature dependence of the two red2 substates

The temperature dependence of the induction of this new signal is illustrated in Fig. 3, which shows a series of CW EPR spectra measured at W-band frequencies (−213 °C).

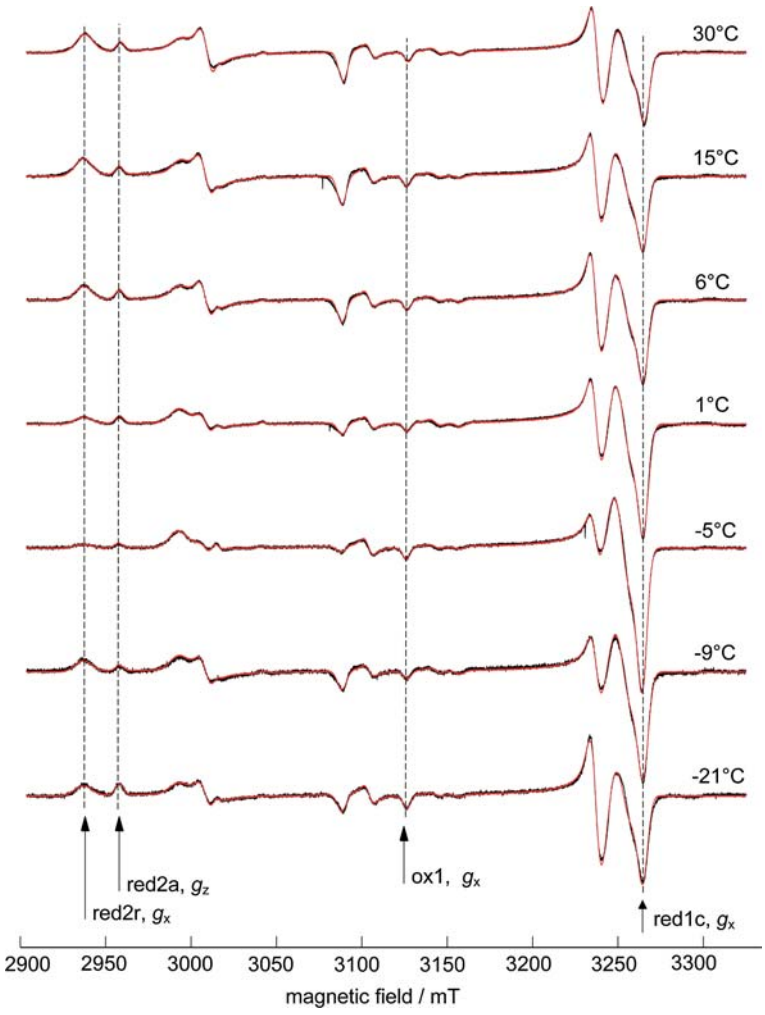

Fig. 3 CW EPR spectra (*black lines*) and spectral simulations (*red lines*) of MCR red1/red2 at W-band (approximately 94 GHz) and at −213 °C as a function of the incubation temperature before freeze–quenching the sample. The temperature dependence of the content of the individual species is clearly visible. The ox1 species serves as an internal standard as its absolute content does not depend on the induction temperature

Before the samples were frozen according to the procedure described in the "Materials and methods," the thin, sealed sample tubes were held at a certain temperature (indicated in the spectra) for 4 min. We deliberately chose to follow this procedure since fluid aqueous samples like MCR strongly absorb microwaves, which reduces the quality factor of the resonator and makes it tedious to achieve sufficient signal-to-noise ratio. This is a serious impediment when measuring full series of temperature-dependent CW EPR spectra at high-field. Assuming that the freezing (on the millisecond scale) is fast compared with conformational rearrangements in the enzyme, one can such take a "snapshot" of the enzyme at the incubation temperature before freezing. Previous studies have given a good indication that for forming MCR-red1/red2 the binding of HS-CoB is the rate-determining step, which is slow compared with the freeze–quench times in our approach.

Figure 3 also shows the optimized simulations (red lines) of the respective spectra: these simulations are the weighted sum of the six component spectra (Fig. 2) and the main variables in the optimization are the relative weights that each component contributes to the overall spectrum. The integral of an EPR absorption spectrum (i.e., the double-integral of a CW EPR spectrum) is a direct measure of the number of contributing spins. Hence, the *relative* weight w_i that the spectrum V_i of each component i contributes to the spectrum is a direct measure of the *relative* amount of spins that this component contributes. The complete spectral simulation V_{sum} can thus be described as

$$V_{\text{sum}} = \sum_i w_i V_i, \qquad (2)$$

where the sum over all weights was normalized to unity. Therefore, the respective value for w_i reveals the percentage that component i contributes. In this context, the relative weight of the ox1 signal is a very good internal standard since the *absolute* amount of ox1 signal did not change with different temperatures prior to freezing. By analyzing the optimized simulations in terms of the relative contribution of each individual spectral component, we can thus obtain direct insight into the temperature-dependent induction of the respective MCR states.

In the series of spectra in Fig. 3, several trends of temperature dependence are observable. Just following one feature of each of the signals of interest (indicated by dashed lines) it becomes apparent that—starting at the spectrum for −5 °C—the red1c signal decreases,while both red2 signals, red2a and red2r, increase with increasing temperature.

To quantitatively analyze the temperature-dependent induction of signals, we followed the normalized weights of each spectral component (after subtracting the probehead background signal) as a function of the incubation temperature before freezing. This is plotted in Fig. 4.

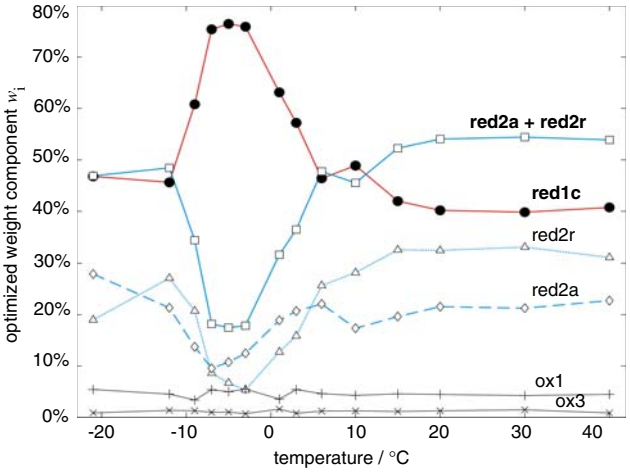

Fig. 4 Dependence of the relative weights of the individual EPR-active components of MCR. The optimized weights shown here were obtained after subtraction of the background signal and normalization to unity. The weights were not corrected for the approximately 25% EPR-silent MCR (Ni^{II}) known to be present

As described above, the spectral contributions of both ox components, ox1 and ox3, remains constant throughout the whole temperature range from −21 to 40 °C and thereby indicates the viability of our approach. The fact that in a sealed and degassed sample tube the amount of ox species—1.5% for ox3 and 4.5% for ox1—remains constant where oxygen, which can induce ox states, is excluded also shows that these states are not affected by the conversion of red1c to the red2 states.

Unlike in the previous X-band study we have explicitly included incubation temperatures below 0 °C. We will first discuss the trends starting at a minimum temperature of −7 °C and will later explain the behavior below this temperature.

The trend for the red1c species (Fig. 4) qualitatively correlates with previous findings that the red1c signal is largest at temperatures below 20 °C. We find that between −7 and −3 °C the red1c signal reaches its maximum and amounts to 76% of the total. Between −1 and 20 °C the relative weight w_{red1c} decreases, first steeply and then it levels off to its minimum value of 40% above 20 °C.

The two individual components red2a and red2r (Fig. 4) have similar temperature dependences and both show the opposite behavior from red1c. Between −7 and −3 °C both red2 states have their minimum values with w_{red2a} = 9–12% and w_{red2r} = 9–6%. Between −3 and 15 °C both w_i curves rise, with the red2r increase being more pronounced. At temperatures above 15 °C both signal contributions level off to a maximum induction of w_{red2a} = 22% and w_{red2r} = 32%. It is interesting to note that

below 6 °C the red2a component has a higher contribution to the signal than red2r. It is also apparent that the absolute minimum for red2a is reached at −7 °C, while for red2r this temperature is −3 °C. Whether this difference is significant has to remain open at present, although we have repeated these measurements several times and only found slight variations of the extracted weights. Certainly, the trends for red2a and red2r run in parallel, and in Fig. 4 we therefore also plotted the summed weights of red2r and red2a squares/full blue line).

The trend of the sum "red2a + red2r" complements the red1c trend, being mirrored at 47%.

A striking observation was made at incubation temperatures below −7 °C. The spectral contribution of red1c decreased down to 47% (at −21 °C), while the combined red2 contributions increased to 47% (at −21 °C). To investigate this somewhat peculiar low temperature behavior, CW EPR measurements (X-band, approximately 9.4 GHz) were performed at the incubation temperatures (Fig. S1). As mentioned above, we could not perform such "real temperature measurements" at W-band frequencie-sowing to difficulties with measurements of aqueous samples at high field/high frequency. In these X-band CW EPR measurements we gradually decreased the temperature and recorded the EPR spectra. Qualitatively, the temperature-dependent differences of the spectra are clearly observable and confirm that the red2a content increases again significantly below −7 °C.

The reproducibility of the determined component weights was excellent for 30 and 40 °C (within 1–2 wt% deviation). At lower temperatures the reproducibility is not as good (within 1–9 wt% deviation), but the trend was always confirmed. This shows that this is not merely an artifact caused by an inhomogeneous quench–freeze of the samples and will be the first topic discussed in the next section.

Discussion

Increase of red2-type state content below −7 °C

Our sample—a mixture of the enzyme and the aqueous buffer—is expected to have a melting/freezing temperature at slightly lower temperatures than 0 °C. The abrupt reversal of the w_i versus incubation temperature curves at −7 °C indicates that this is the actual freezing point. In our sample preparation procedure (see "Materials and methods") we first thawed the sample to room temperature and then incubated it in a temperature bath having a certain temperature, e.g., −9, −21°C. Bearing this in mind, one could envision two reasons for the reappearance of the red2-type states in the EPR spectra of samples incubated below the freezing point. If, by putting the tube in the low-temperature bath, a freeze–quench process takes place (with a much less steep temperature gradient of only −30 to −40 °C), this observed phenomenon would merely be an artifact caused by the incubation procedure. As described before, we tested this by performing X-band CW EPR measurements (Fig. S1), in which the sample was certainly cooled down to thermal equilibrium with the surroundings. Since these measurements clearly prove a reappearance of the red2-type states at low temperatures when cooling down slowly, we interpret this phenomenon as a response of the system and not as an artifact. Owing to the small temperature change when the sample tube is inserted in the incubation bath, the sample seems to have reached its incubation temperature in equilibrium with the surroundings.

In the case of cooling in equilibrium, the enzyme has to adapt to the external pressure exerted by freezing (and expanding) water and possible changes in local concentration, pH, ionic strength and even redox potential when water is crystallizing out. The external stress may well trigger such conformational changes in the enzyme that force HS-CoM and HS-CoB to induce the red2-type states again, mimicking the actual thermodynamic induction at temperatures above 20 °C. MCR could thus be seen to go into a low-energy *resting state* upon freezing. This resting state could help the enzyme retain its reactivity for higher temperatures and survive the freezing. This leads to the question why the amounts of red1c and red2-type (red2a and red2r) signals are equal for incubation temperatures below −7 °C. If the complex changes in the freezing matrix induce the increase of red2 components, it is highly unlikely that the enzyme surroundings will be heterogeneous in such a way that approximately 50% of the molecules are in surroundings inducing 100% red1c signal and approximately 50% of the molecules are in surroundings inducing 100% red2-type signals. It is far more likely that all the enzyme molecules have similar interactions with the surrounding matrix. Therefore, the induction of red1c and red2-type states at almost equal percentages may actually be a consequence of the proposed *half-of-the-sites reactivity* [8]. One of the two active sites could adopt the red2r state and by the linkage through the enzyme backbone force the other site to adopt the red1c or the red2a state or vice versa (an explanation for the possible pairs is given in the next section).

Temperature-dependent conversion of red1c to the red2-type states

Analysis of the temperature series above −7 °C gives some insight into structural changes occurring in MCR during

the conversion of the red1c state to the red2 states. The red1c and red2r states, respectively, have been characterized with advanced pulse EPR methods in previous studies [19, 20]. The red2r state was found to have the sulfur of HS-CoM bound axially from the top to the nickel of F_{430}.

The discovery of the red2a state may eventually give hints on how exactly the red1c state is converted upon binding of HS-CoB. red2a and red2r have a similar temperature dependence, with that of red2r being more pronounced. Both components are only observed in the presence of HS-CoB. Several conversion pathways are possible: red2a may be an intermediate state in the conversion of red1c to red2r, or red2r may be an intermediate in the conversion of red1c to red2a, or the states may compete with each other, as described by the following equations:

$$\text{red1c} \underset{\text{-HS-CoB}}{\overset{\text{+HS-CoB, }\Delta T}{\rightleftharpoons}} \left[\text{red2a} \rightleftharpoons \text{red2r}\right] \tag{3a}$$

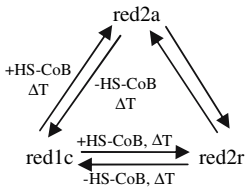

(3b)

A further discrimination between the Eqs. 3a and 3b describing the changes in the active site triggered by the addition of HS-CoB and thermal energy is not possible with the data presently available.

The last topic to be discussed is the observation that at temperatures above 20 °C the combined red2 states can be induced to an amount of 54% of the overall signal, while the red1c signal only totals 40%. To exclude sample-specific features we repeated these experiments several times with other MCR-red1/red2 samples but always found similar optimized component weights. It was never possible to achieve a *significantly higher* conversion than 50% of the combined red2 states. However, when discussing the significance of relative weights of the individual components, one has to consider that our samples contained an estimated 25% of the active sites in the EPR-silent (Ni^{II}) form. We tested whether depending on the temperature conversion of active sites of MCR to EPR-silent (Ni^{II}) form takes place. We did so by performing a numerical double integration of the CW EPR signals and comparing those numbers. The double-integral of a CW EPR spectrum is a direct measure of the absolute amount of observed spins. We found that independent of the incubation temperature the overall double-integral (normalized to the number of scans etc.) only varies by less than 5% around a mean value of $(6.25 \pm 0.25) \times 10^8$, which lies well within the experimental variation and indicates that no conversion to or from EPR-silent forms takes place. In the latter case, a significantly larger variation and in particular a temperature dependence should have been observed.

Our finding that the combined red2 states can be induced to slightly more than 50% of the EPR-active states does not contradict the proposed half-of-the-sites reactivity for MCR. An alternative explanation could be that the half-of-the-sites reactivity picture may hold true for the red2r state only. This means that if one site is in the red2r state its partner site may be in either the red1c or the red2a state. Additionally, a site in the red2a state might, just like the red1c state, be able to have an intramolecular partner site that is in the red1c, red2a or red2r state. These pair relationships would then not contradict the half-of-the-sites reactivity for MCR since the maximum amount of red2r is significantly lower than 50%.

Conclusions and outlook

We reported for the first time that the red2 state of MCR actually consists of two substates, which are designated red2r for the state with a rhombic CW EPR signal and red2a for the state with an axial CW EPR spectrum. The CW EPR signal of red2a is similar to that of red1c but its induction increases with temperature similar to that of red2r. The observation that the weights of the two red2 states increase despite the low temperature when the sample is slowly frozen in thermal equilibrium indicates that factors other than temperature, such as the complex changes in the freezing matrix, are able to induce the red2r and red2a states to up to 50%. In this manner, the enzyme could alleviate the external stress exerted by these complex changes in the freezing matrix.

It is necessary to further investigate the newly found red2a component to discriminate between the possible induction shown in Eqs. 3a and 3b. Such a characterization could be achieved by pulse EPR methods like pulse electron–nuclear double resonance and HYSCORE, possibly in combination with selective isotope labeling and kinetic freeze–quench experiments. Such studies are currently on their way in our laboratories.

Acknowledgements We thank the Swiss National Science Foundation (SNF) and the Fonds der Chemischen Industrie for financial support. D.H. gratefully acknowledges a research scholarship (HI 1094/1-1) from the Deutsche Forschungsgemeinschaft (DFG).

References

1. Thauer RK (1998) Microbiology 144:2377–2406
2. Thauer RK, Jungermann K, Decker K (1977) Bacteriol Rev 41:100–180

3. Ermler U, Grabarse W, Shima S, Goubeaud M, Thauer RK (1997) Science 278:1457–1462
4. Goubeaud M, Schreiner G, Thauer RK (1997) Eur J Biochem 243:110–114
5. Pelmenschikov V, Blomberg MRA, Siegbahn PEM, Crabtree RH (2002) J Am Chem Soc 124:4039
6. Kunz RC, Horng YC, Ragsdale SW (2006) J Biol Chem 281:34663–34676
7. Mahlert F, Grabarse W, Kahnt J, Thauer RK, Duin EC (2002) J Biol Inorg Chem 7:101–112
8. Goenrich M, Duin EC, Mahlert F, Thauer RK (2005) J Biol Inorg Chem 10:333–342
9. Wasserfallen A, Nolling J, Pfister P, Reeve J, Conway de Macario E (2000) Int J Syst Evol Microbiol 50(Pt 1):43–53
10. Gunsalus RP, Romesser JA, Wolfe RS (1978) Biochemistry 17:2374–2377
11. Kobelt A, Pfaltz A, Ankel-Fuchs D, Thauer RK (1987) FEBS Lett 214:265–268
12. Ellermann J, Hedderich R, Böcher R, Thauer RK (1988) Eur J Biochem 172:669–677
13. Rospert S, Linder D, Ellermann J, Thauer RK (1990) Eur J Biochem 194:871–877
14. Bonacker LG, Baudner S, Mörschel E, Böcher R, Thauer RK (1993) Eur J Biochem 217:587–595
15. Duin EC, Signor L, Piskorski R, Mahlert F, Clay MD, Goenrich M, Thauer RK, Jaun B, Johnson MK (2004) J Biol Inorg Chem 9:563–576
16. Mahlert F, Bauer C, Jaun B, Thauer RK, Duin EC (2002) J Biol Inorg Chem 7:500–513
17. Bradford MM (1976) Anal Biochem 72:248–254
18. Stoll S, Schweiger A (2006) J Magn Reson 178:42
19. Finazzo C, Harmer J, Bauer C, Jaun B, Duin EC, Mahlert F, Goenrich M, Thauer RK, Van Doorslaer S, Schweiger A (2003) J Am Chem Soc 125:4988–4989
20. Finazzo C, Harmer J, Jaun B, Duin EC, Mahlert F, Thauer RK, Van Doorslaer S, Schweiger A (2003) J Biol Inorg Chem 8:586–593